Numerical simulation of continuously regenerating diesel particulate filter

by

Kazuhiro YAMAMOTO and Kazuki YAMAUCHI
Department of Mechanical Science and Engineering, Nagoya University
Furo-cho, Chikusa-ku, Nagoya, Aichi 464-8603, JAPAN

ABSTRACT

In many countries, stricter exhaust emission standards are being set, and a diesel particulate filter (DPF) has been used to trap particulate matters (PM) including soot in diesel exhaust gas. It is reported that DPF filling with PM causes higher back-pressure and more fuel consumption, and continuously regenerating DPF is needed. Usually, to reduce the soot oxidation temperature, a catalyzed DPF is used. However, the phenomena inside DPF are not well understood, because it is difficult to conduct measurements inside the filter. In this study, we simulated soot oxidation and deposition by the lattice Boltzmann method to observe the transport process in continuously regenerating DPF. The inner structure of the filter was obtained by an X-ray CT technique. The reaction rate of soot oxidation by the Pt catalyst, as well as soot deposition probability in the numerical model, was evaluated in experiments. The soot trap and oxidation were investigated to discuss the conditions for the continuous regeneration. When the filter temperature (Tw) is 600 K, the amount of deposited soot is quite similar to that without considering the soot oxidation, so that the soot is not oxidized at this temperature. When Tw is raised to be 800 K, the amount of deposited soot is saturated. Thus, at Tw = 800 K or higher, the filter clogging can be avoided to achieve the continuous regeneration.

1. Introduction

Diesel passenger vehicles have been widely used especially in European countries. Compared with gasoline counterparts, they have good features of high torque at low speed, excellent durability and reliability, higher tolerance to fuel properties, and better fuel efficiency [1]. The main problem with diesel vehicles is that they produce particulate matters (PM) including soot in exhaust gas [2, 3]. PM is a serious atmospheric pollutant and has also been linked to carcinogenicity [4], and diesel emissions and control are still very much in the forefront [3, 5]. As one of the key technologies, a diesel particulate filter (DPF) for the after-treatment of the exhaust gas has been developed [5-7].

Figure 1 shows a schematic of DPF. Upper figure shows PM trap inside porous filter wall. Typically, the ceramic DPF has a honeycomb structure, with alternate closure of inlet and outlet channels. The mechanism for PM trap is simple: when the exhaust gas passes through the filter wall, PM is trapped, so that the soot cake is formed on the surface of filter substrate, which is orange area in this figure. Then, the filter would be plugged with PM to cause an increase of filter backpressure [8, 9]. If the backpressure is high, the engine may stall or the fuel consumption increases. In order to prevent these disadvantages, the filter must be regenerated by oxidizing PM. However, the temperature of diesel exhaust gas is not high enough for soot oxidation [5, 6,

10]. In addition, DPF may be eroded due to the heat generated in PM oxidation process. Therefore, PM must be oxidized at low temperatures by keeping high filtration for PM trap.

Fig.1

The system where PM is trapped and oxidized simultaneously is called a continuously regenerating DPF [3,5]. A catalyst, which adheres to the surface of the ceramic filter substrate, is usually used to reduce the PM oxidation temperature. However, the thermal durability of existing platinum catalyst-supported DPF is inadequate, which means that the catalyst may be damaged by PM oxidation and the filter substrate may also be cracked. In addition, since platinum is a rare metal, the amount of catalyst must be suppressed. Then, a full investigation of exhaust gas flow, PM deposition, and PM oxidation in the continuously regenerating DPF is needed. Although a challenging to visualize the processes of PM oxidation and deposition has been conducted experimentally [11, 12], it is still difficult to observe the phenomena inside DPF. So far, we have proposed a numerical scheme for the simulation of DPF by the lattice Boltzmann method (LBM) [13-17].

In the present paper, we simulate the deposition and oxidation processes of soot in the continuously regenerating DPF. To obtain the information of an actual filter, the inner structure of a cordierite DPF with a Pt catalyst is obtained by an X-ray computer tomography (CT) technique. The tomography-assisted simulation is conducted to understand the deposition and oxidation processes in DPF.

2. Numerical analysis

2.1. Lattice Boltzmann method

The lattice Boltzmann method (LBM) used in the simulation is the simplification of Boltzmann equation [18]. The LBM analyses the flow based on the movement and collision processes of artificial particles moving at lattice nodes. However, the LBM does not consider each particle; instead, it uses a distribution function on the basis of the average particle motions. The distribution function of particles is determined by the translational process, in which the distribution function moves from one lattice node to another at one time step, and by the collision process, in which the distribution function is relaxed to the equilibrium distribution due to collision. The model of D3Q15 using cubic lattices is usually used for 3D calculation [19].

As for the combustion simulation, we followed the same numerical scheme proposed in our previous study [20]. The flow field was determined using the distribution function of pressure, *p*. The evolution equation and the equilibrium distribution function are expressed as follows:

$$F_{p,\alpha}(\vec{x}+\vec{e}_\alpha\delta_t, t+\delta_t) - F_{p,\alpha}(\vec{x},t) = -\frac{1}{\tau_p}[F_{p,\alpha}(\vec{x},t) - F^{eq}_{p,\alpha}(\vec{x},t)] \qquad (1)$$

$$F_{p,\alpha}^{(eq)} = w_\alpha \left\{ p + p_0 \left[3\left(\frac{\vec{e}_\alpha \cdot \vec{u}}{c^2} \right) + \frac{9}{2}\left(\frac{\vec{e}_\alpha \cdot \vec{u}}{c^2} \right)^2 - \frac{3}{2}\left(\frac{\vec{u}}{c} \right)^2 \right] \right\} \qquad (2)$$

where δ_t is the time step, τ is the relaxation time which controls the rate of approach to equilibrium, and $\vec{e}_\alpha$ (α = 1 - 15) is the unit vector of D3Q15 model in lattice space. The constants in Eq. (2) are $w_{1\text{-}6}$=1/9, $w_{7\text{-}14}$=1/72, and w_{15}=2/9. The pressure p and the local velocity of $\vec{u}$ = (u, v, w) are obtained using the low Mach number approximation [20] as follows:

$$p = \sum_\alpha F_{p,\alpha} \qquad (3)$$

$$\vec{u} = \sum_\alpha \frac{F_{p,\alpha}}{P_{out}} \cdot \frac{T_0}{T} \vec{e}_\alpha \qquad (4)$$

where P_{out} represents atmospheric pressure. The kinematic viscosity of ν in LBM is related with the relaxation time of τ, using the following formula:

$$\nu = \frac{2\tau_p - 1}{6} \frac{\delta_x^2}{\delta_t} \qquad (5)$$

Through the Chapman-Enskog procedure, the Navier-Stokes equations are derived from these equations [18]. In the calculation, all of the variables were set to be dimensionless, and the same dimensionless quantities such as the Reynolds number (Re = $U_{in}W / \nu$) were used in LBM [20], where U_{in} is the inlet velocity of exhaust gas, W is the width of numerical domain in **Fig. 3**.

Similar to the flow field, the scalar quantities of temperature and species concentrations were also determined by their distribution functions [13, 14, 20]. The evolution equation and the equilibrium distribution function for the scalar quantities are expressed as follows:

$$F_{s,\alpha}(\vec{x}+\vec{e}_\alpha\delta_t, t+\delta_t) - F_{s,\alpha}(\vec{x},t) = -\frac{s}{\tau_s}[F_{s,\alpha}(\vec{x},t) - F_{s,\alpha}^{(eq)}(\vec{x},t)] + w_\alpha Q_s \qquad (6)$$

$$F_{s,\alpha}^{(eq)}(\vec{x},t) = w_\alpha s\left\{1 + 3\left(\frac{\vec{e}_\alpha\cdot\vec{u}}{c^2}\right) + \frac{9}{2}\left(\frac{\vec{e}_\alpha\cdot\vec{u}}{c^2}\right)^2 - \frac{3}{2}\left(\frac{\vec{u}}{c}\right)^2\right\} \qquad s = T, Y_i \qquad (7)$$

where s is the value of temperature and mass fraction of species i, and Q_s represents the source term due to the chemical reaction in the soot oxidation process. The procedure to evaluate the catalytic reaction will be explained later. As for the reaction of soot in gas phase, an overall one-step reaction of $C + O_2 \rightarrow CO_2$ was

used [13, 14, 21]. For relaxation time of τ_s, which is required for calculating the concentration and temperature fields, the same value as that of τ_p in Eq. (5) was used. The temperature and the mass fraction of species *i* (mass fraction) are obtained as follows:

$$T = \sum_{\alpha} F_{T,\alpha} \qquad (8)$$

$$Y_i = \sum_{\alpha} F_{Y_i,\alpha} \qquad (9)$$

2.2. Soot deposition model

In this section, a soot deposition model is explained. Generally, the soot has complex geometry of nanoparticles [2, 22, 23]. Since the size of diesel soot has a nano-scale, it is difficult to realize the deposition phenomenon of soot particles precisely. Then, the soot deposition is described by the modified particle deposition model [24]. Different from Lagrangian approach through the equation of motion, individual particles were not considered. Instead, the soot concentration was monitored. The mass fraction of deposited soot is given by

$$Y_{C,s}(\boldsymbol{x},\ t+\delta_t) = \sum_{\alpha} F_{C,\alpha}(\boldsymbol{x},\ t)\cdot P_D + Y_{C,s}(\boldsymbol{x},\ t) \qquad (10)$$

where $Y_{C,s}$ is the mass fraction of deposited soot of solid phase, and P_D is the soot deposition probability, which controls the amount of soot attached to the filter substrate [15, 17]. If P_D is unity, soot is thoroughly deposited on the filter without reflection. Else, a part of soot is bounced back and transported downstream. As the soot deposition is continued, the soot mass fraction sometime becomes unity. When this limit is reached, the solid site is piled up, and the deposited soot region is treated as non-slip wall, which implies a change of boundary condition for fluid. In this study, we experimentally determined the value of P_D.

2.3. Numerical domain

In this study, the catalyzed cordierite DPF was considered. In the simulation, we used the internal structure of DPF obtained by the X-ray CT technique. **Figure 2** shows DPF structure in *yz* plane, which is the cross section at the center of DPF. The exhaust gas passes through the filter wall in *x* direction, and the image size of **Fig. 2** is 661 μm (*y*) × 661 μm (*z*). The spatial resolution was 1.15 μm/pix, which was the grid size in the simulation. The cell density of DPF is 300 cpsi, and its wall thickness is 263 μm. The average porosity is

about 0.59. As seen in this figure, the filter has very complex structure with many pores. In the tomography-assisted simulation, a part of CT data was used.

Fig.2

Figure 3 shows the numerical domain. The filter structure obtained by the X-ray CT is placed at the center of the numerical domain. The width of the numerical domain is W. In the preliminary simulation, W was varied to determine the proper numerical domain. As W was increased, the pressure drop across the filter wall became smaller. At $W > 46$ μm, the pressure drop was saturated. Then, W was set to be 46 μm in the simulation. The total size is 330 μm (x) × 46 μm (y) × 46 μm (z), including inlet and outlet zones of 34 μm. The number of lattices is 290 × 41 × 41.

Fig.3

Next, the boundary conditions are explained [13-17]. At filter inlet, the exhaust gas containing soot was evenly flowed from the upstream. The flow velocity at the inlet (U_{in}) was set at 0.03 m/s, which was the value in experiments. The temperature of exhaust gas at the inlet (T_{in}) was set at 350 ºC. The exhaust gas was composed of soot, oxygen, and nitrogen. The oxygen concentration was 8% in the volume fraction (X_{O2}), and soot mass fraction was 1.6×10^{-4} ($Y_{c,in}$), which was the experimental value on an engine test bench. It was the high loaded condition, because the continuous regeneration must be achieved even under high loaded case. The velocities were set at $u = U_{in}$, $v = 0$, and $w = 0$. At four side walls, the slip boundary was adopted based on

the assumption of symmetry. At the outlet, the pressure was constant (atmospheric pressure), and the gradient of scalar such as temperature and mass fraction was set to be zero. The non-slip boundary was adopted at the surface of the filter substrate or the deposited soot layer.

3. Results and discussion

3.1. Soot oxidation rate with catalyst

Firstly, the soot oxidation rate with catalyst was evaluated. The catalyst was uniformly adhered to the surface of the filter substrate. The soot reaction rate was obtained based on data in engine test bench equipped with the catalyzed DPF [9,17]. **Table 1** shows the engine specifications. Here, the experimental procedure was explained. Initially, some amount of diesel soot was trapped inside DPF. Then, the temperature was increased for the filter regeneration. By measuring the emissions of CO and CO_2, the mass of reacted soot was calculated. The soot oxidation rate was assumed as the first-order reaction of the soot concentration (soot mass) with the following Arrhenius type equation [14]:

Table1

$$-\frac{dm}{dt} = km, \qquad k = A\exp\left(-\frac{E}{RT}\right) \qquad (11)$$

where m represents the mass of unreacted soot inside DPF, k represents a reaction rate coefficient, A represents a pre-exponential factor, E represents activation energy, and R represents the gas constant. Based on the Arrhenius plots, the frequency factor was 5.92×10^9 1/s, and activation energy was 184 kJ/mol.

3.2. Determination of soot deposition probability

As explained in section 2.2, we need to determine the deposition probability of P_D. We monitored the time-variation of deposited soot in engine test bench [17]. The exhaust gas temperature was controlled to be below the soot oxidation temperature. On the other hand, numerical simulations were conducted by varying P_D, compared with experimental results. According to the experiments, only soot deposition was considered in the simulation. **Figure 4** shows the simulated filtration efficiency of η at P_D = 0.0001, 0.001, 0.002, 0.003, 0.005, 0.01, 0.1, and 1.0, defined as follows:

$$\eta = \frac{Inlet\ soot\ mass\ fraction - Outlet\ soot\ mass\ fraction}{Inlet\ soot\ mass\ fraction} \qquad (12)$$

When $P_D \geqq 0.01$, the filtration efficiency is almost 100%: i.e., there is no soot leakage passing through the filter. When $P_D = 0.001$, η is about 50%: i.e., only half of soot in the exhaust gas is trapped, and another 50% flows out.

Fig.4

It should be noted that, when a large amount of soot is deposited inside DPF, the soot layer is formed on the surface of the filter inlet [8, 9, 14], and consequently, the filtration efficiency increases. Thus, in order to determine the soot deposition probability, the initial filtration efficiency before the soot layer formation was evaluated in experiments. It was found that the initial filtration efficiency was 70%, equivalent to the numerical result at $P_D = 0.002$. Interestingly, this value is very close to the previous study using a metal filter [17]. In the next section, simulation results of the continuously regenerating DPF were shown, using $P_D = 0.002$.

3.3. Combustion field and deposited soot region

To explain the continuously regenerating DPF, the typical soot profile inside DPF is shown in **Fig. 5**, which is 3D distribution of soot mass fraction in gas phase at $t = 3.833$ s. Time is counted after starting the

simulation. The filter temperature of T_W is 1000 K, which is the temperature of the filter substrate. Three color surfaces correspond to the contour of soot in gas phase, and the gray region corresponds to the filter substrate. 2D profile of soot mass fraction in *xy* plane is also shown. It is seen that the amount of soot in gas phase is largely decreased around the filter inlet, expectedly caused by the soot deposition and oxidation. Later, the detailed discussion will be made.

Fig.5

Next, the formation of soot deposition region was investigated. **Figure 6** shows the soot deposition regions at T_W = 600, 800, and 1000 K, obtained at t = 3.833 s. In this figure, the black region indicates the soot deposition layer on the surface of the filter substrate, where the mass fraction of deposited soot, $Y_{c,s}$, is over 0.001. In this figure, 2D profile in *xy* plane at the center (z = 0.023 mm) shows the distribution of soot mass fraction in gas phase. It is found that the deposited soot region is decreased as the filter temperature is increased. Especially, at T_W = 1000 K, there is no deposited soot. That is, when the filter temperature is increased, the soot oxidation is largely promoted. Resultantly, even if the soot in gas phase is deposited on the surface of the filter substrate, the deposited soot is instantly oxidized with catalyst. This situation is ideal to realize the continuously regenerating DPF.

Fig.6

Figure 7 shows distributions of soot mass fraction in gas phase ($Y_{c,g}$), temperature, mass fraction of

deposited soot ($Y_{c,s}$), and the reaction rate. Each profile is shown in *xy* plane at z = 0.023 mm. The filter temperature is T_W = 600 K, obtained at t = 3.833 s. It is seen that the soot concentration in gas phase is gradually decreased inside the filter. Some leakage of soot is observed at the filter outlet. There is a large layer of deposited soot, which covers the filter substrate in the entire domain. The temperature inside the filter was uniform, and the reaction rate is high on the surface of the filter substrate. Therefore, it is considered that the soot is firstly deposited on the surface of filter substrate, and then, the deposited soot is oxidized by the catalyst.

Fig.7

For comparison, results at T_W =1000 K are shown in **Fig. 8**. When the filter temperature is increased, the soot oxidation is promoted. As seen in **Fig. 8a**, less soot in gas phase is observed. Different from the profile in **Fig. 7a**, there is no soot at the filter outlet. In **Fig. 8c,** the deposited soot is still observed at the upstream section of the filter, but that amount is very small. As seen in **Fig. 8d,** the reaction rate is extremely high at the filter substrate with catalyst. The maximum reaction rate is 50 times larger than that at T_W= 600 K. Thus, at T_W =1000 K, most of deposited soot is instantly oxidized, so that the soot layer cannot grow.

Fig.8

3.4. Soot deposition profile and conditions for continuously regenerating DPF

Finally, conditions for the continuously regenerating DPF were examined. **Figure 9** shows the profile of deposited soot inside DPF along *x*-axis, which is the averaged soot mass fraction in *yz* plane. The filter temperature of T_W was varied from 600 to 1000 K. For comparison, the simulation without soot oxidation was conducted to discuss the effect of soot deposition only. It is seen that, at T_W = 600 K, soot is deposited on the entire surface of the filter substrate, and the amount of deposited soot is extremely high at the filter inlet. Since the profile of deposited soot at T_W = 600 K matches the simulation result without the soot oxidation, the soot oxidation seldom occurs at this temperature. That is, the reduction of soot concentration in gas phase is caused only by the soot deposition. As the filter temperature is higher, more soot is burned inside DPF. Deposited soot is nearly zero at T_W = 1000 K.

Fig.9

Figure 10 shows the time-variation of deposited soot inside DPF. The filter temperature was changed from 600 K to 1000 K. Needless to say, as the soot oxidation rate is high enough; the amount of deposited soot is not increased. In this case, the filter is not expected to be clogged by the deposited soot. It is seen that the amount of deposited soot increases linearly at T_W = 600 K, corresponding to the result without soot oxidation. Therefore, it is confirmed that the soot cannot be oxidized at T_W = 600 K. At T_W = 800 K, the amount of deposited soot is almost saturated after t = 3 s. At T_W = 1000 K, the amount of deposited soot is

almost zero. Therefore, the presence of catalyst enables the complete regeneration [6, 25], and at T_W = 800 K or higher, the filter clogging can be avoided to achieve the continuous regeneration. In future, the soot oxidation process will be examined in the variety of mixtures to consider any situations of the continuous regeneration.

Fig.10

4. Conclusions

In the present study, the continuously regenerating DPF was simulated by the lattice Boltzmann method, using the inner structure of the real cordierite DPF. The processes of soot deposition and oxidation were discussed by varying the filter temperature, and conditions for the continuous regeneration were examined. The following conclusions were drawn.

1. The reaction rate of soot oxidation with the Pt catalyst was evaluated. The Arrhenius equation for the first-order reaction was adopted. Consequently, the pre-exponential factor was 5.92×10^9 1/s and the activation energy was 184 kJ/mol.
2. The soot deposition probability was determined experimentally. By comparing the initial filtration

efficiency obtained in numerical results, the soot deposition probability of P_D was 0.002.

3. When the filter temperature is 600 K, the amount of deposited soot is quite similar to that without considering the soot oxidation, so that the soot is not oxidized at this temperature. When the filter temperature is raised to be 800 K, the amount of deposited soot is saturated. Thus, at T_W = 800 K or higher, the filter clogging can be avoided to achieve the continuous regeneration.

Acknowledgments

This work was partially supported by the Rare Metal Substitute Materials Development Project, New Energy and Industry Technology Development Organization (NEDO) in Japan.

References

[1] A. Yezerets, N. W. Currier, et al., *Applied Catalysis B* 61 (2005) 120-129.

[2] D. B. Kittelson, *Journal of Aerosol Science* 29 (1998), 575-588.

[3] T. V. Johnson, *SAE Technical Paper* 2010-01-0301 (2010) 16-29.

[4] I. M. Kennedy, Proc. *Combust. Inst.* 31 (2007) 2757-2770.

[5] T. Tzamkiozis, L. Ntziachristos and Z. Samaras, *Atmospheric Environment* 44 (2010), 909-916.

[6] G. C. Koltsakis, A. M. Stamatelos, *Prog. Energy Combust. Sci*. 23 (1997) 1-39.

[7] J. Adler, *International Journal of Applied Ceramic Technology* 2 (2005), 429-439.

[8] E. Wirojsakunchai, et al., *SAE Technical Paper* 2007-01-0320 (2007).

[9] K. Tsuneyoshi, O. Takagi, and K. Yamamoto, *SAE Technical Paper* 2011-01-0817 (2011) 297-305.

[10] H. J. Stein, *Applied Catalysis B* 10 (1996) 9-17.

[11] P. Karin , L. Cui, P. Rubio, T. Tsuruta, and K. Hanamura, *SAE Technical Paper* 2009-01-1476 (2009) 725-733.

[12] G. D. Harvel, J. Chang, A. Tung, P. Fanson, M. Watanabe, *SAE Technical Paper* 2011-01-0599 (2011) 147-157.

[13] K. Yamamoto, N. Takada, and M. Misawa, *Proc. Combust. Inst.* 30 (2005) 1509-1515.

[14] K. Yamamoto, et al., *Proc. Combust. Inst*. 32 (2009) 1965-1972.

[15] K. Yamamoto, et al., *the European Physical Journal* 171 (2009) 205-212.

[16] K. Yamamoto, M. Nakamura, H. Yane, and H. Yamashita, *Catalysis Today* 153 (2010) 118-124.

[17] K. Yamamoto, K. Yamauchi, et al., *Philosophical Transactions A, The Royal Society, London* 369 (2011) 2584-2591.

[18] S. Chen, and G. D. Doolen, *Annual Reviews of Fluid Mech.* 30 (1998) 329-364.

[19] Q. Zou, and X. He, *Physics of Fluids* 9 (1997) 1591-1598.

[20] K. Yamamoto, He, X. and G. D. Doolen, *Journal of Statistical Physics* 107 (2002) 367-383.

[21] K. B. Lee , M. W. Thring, and J. M. Beer, *Combust. Flame* 6 (1962) 137-145.

[22] J. Song, M. Alam, A. L. Boehman, and U. Kim, *Combust. Flame* 146 (2006) 589-604.

[23] K. C. Oh, H. D. Shin, *Fuel* 85 (2006) 615-624.

[24] B. Chopard, A. Masselot, and A. Dupuis, *Computer Physics Communications* 129 (2000) 167-176.

[25] S. Bensaid, N. Russo, *Catalysis Today* 176 (2011) 417-423.

Figure captions

Table 1 Engine specifications.

Fig. 1 A schematic of diesel particulate filter is shown. Upper figure shows PM trap inside porous filter wall.

Fig. 2 DPF structure in *yz* plane of the DPF cross section at the center.

Fig. 3 Coordinate and calculation region are shown. Exhaust gas passes through the filter in *x* direction. A part of CT data was inserted in the numerical domain for tomography-assisted simulation. The width of the numerical domain is *W*.

Fig. 4 Filtration efficiency at different soot deposition probability.

Fig. 5 3D distribution of soot mass fraction at T_W = 1000K is shown. Three color surfaces correspond to the contour of soot in gas phase, and gray region corresponds to the filter substrate.

Fig. 6 Soot deposition region at t = 3.833s is shown by 3D contour; (a) T_W = 600 K, (b) T_W = 800 K, (c) T_W = 1000 K. Soot mass fraction in *xy* plane is also shown.

Fig. 7 Distributions of (a) soot mass fraction in gas phase, (b) temperature, (c) deposited soot, (d) reaction rate at t = 3.833s, T_w = 800 K.

Fig. 8 Distributions of (a) soot mass fraction in gas phase, (b) temperature, (c) deposited soot, (d) reaction rate at t = 3.833s, T_w = 1000 K.

Fig. 9 Distribution of deposited soot at t =3.833 s.

Fig. 10 Time-variation of deposited soot at different filter temperature.

Table 1
Engine specifications

Model	NISSAN YD252
Engine Type	Inline 4-cylinder, DOHC 4 valves
Cylinder head port	Tandem port
Displacement	2488 cc
Maximum power	126 kW @ 4000 rpm
Maximum Torque	403 Nm @ 2000 rpm
EGR System	EGR cooler
Turbocharger system	Variable Geometry Turbo with mechanical control

[Word Count] = (11+2)*7.6 = 99 words

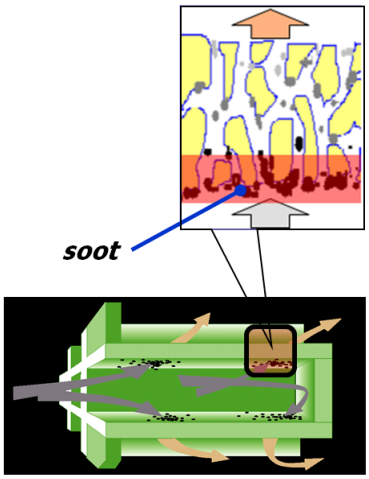

Fig. 1 A schematic of diesel particulate filter is shown.
Upper figure shows PM trap inside porous filter wall.

[Word Count] = (65+10)*2.2*1 + 19 (caption) = 184 words

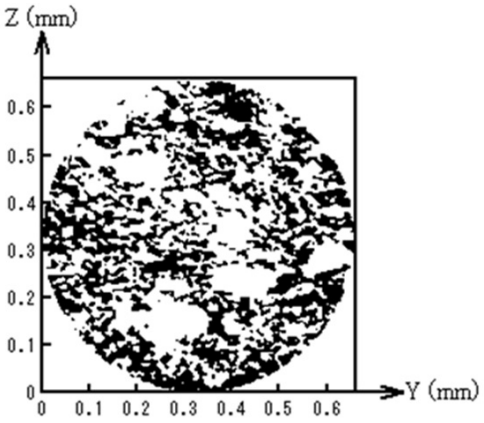

Fig. 2 DPF structure in *yz* plane of the DPF cross section at the center.

[Word Count] = (55+10)*2.2*1 + 15 (caption) = 158 words

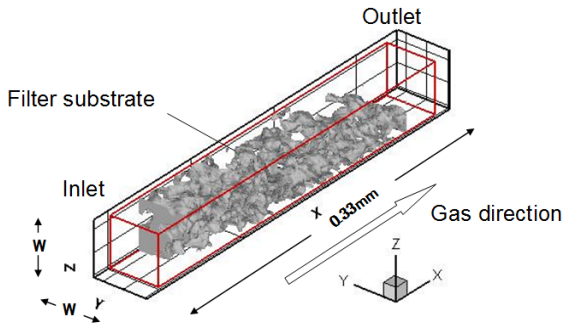

Fig. 3 Coordinate and calculation region are shown. Exhaust gas passes through the filter in *x* direction. A part of CT data was inserted in the numerical domain for tomography-assisted simulation. The width of the numerical domain is *W*.

[Word Count] = (45+10)*2.2*1 + 39 (caption) = 160 words

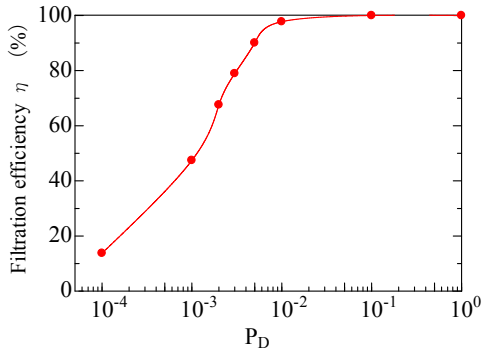

Fig. 4 Filtration efficiency at different soot deposition probability.

[Word Count] = (45+10)*2.2*1 + 9 (caption) = 130 words

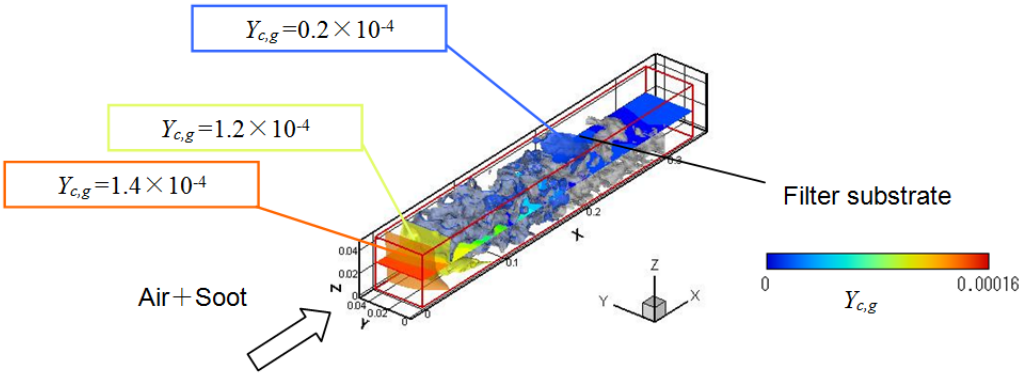

Fig. 5　3D distribution of soot mass fraction at T_W = 1000K is shown. Three color surfaces correspond to the contour of soot in gas phase, and gray region corresponds to the filter substrate.

[Word Count] = (50+10)*2.2*2 + 34 (caption) = 298 words

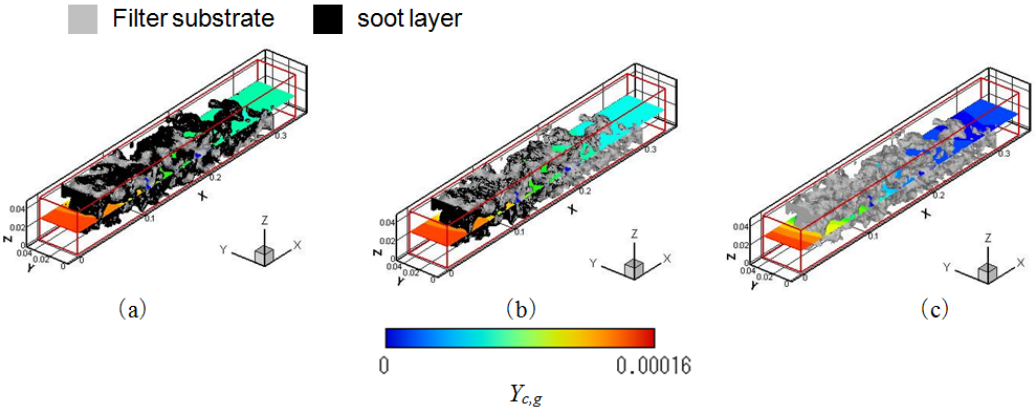

Fig. 6 Soot deposition region at t = 3.833s is shown by 3D contour; (a) T_W = 600 K, (b) T_W = 800 K, (c) T_W = 1000 K. Soot mass fraction in xy plane is also shown.

.

[Word Count] = (50+10)*2.2*2 + 38 (caption) = 302 words

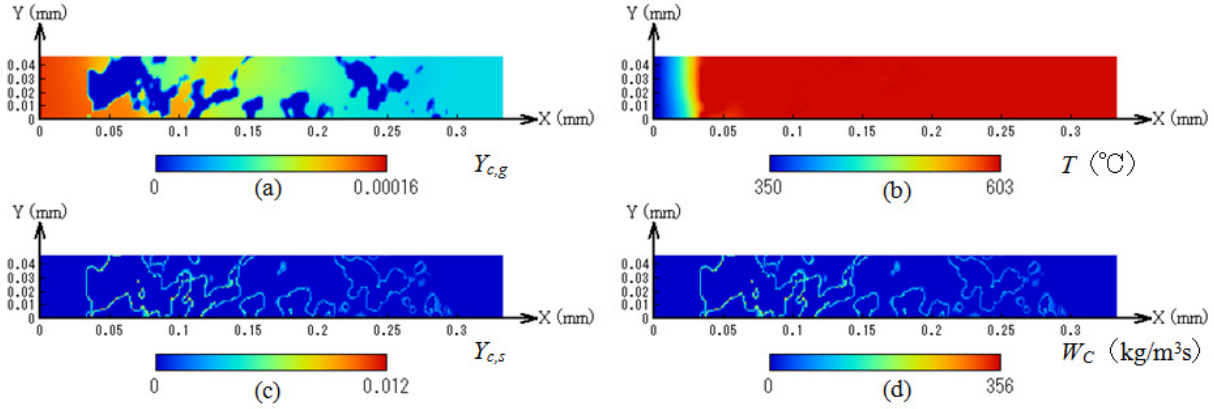

Fig. 7 Distributions of (a) soot mass fraction in gas phase, (b) temperature, (c) deposited soot, (d) reaction rate at t = 3.833s, T_w = 800 K.

[Word Count] = (50+10)*2.2*2 + 27 (caption) = 291 words

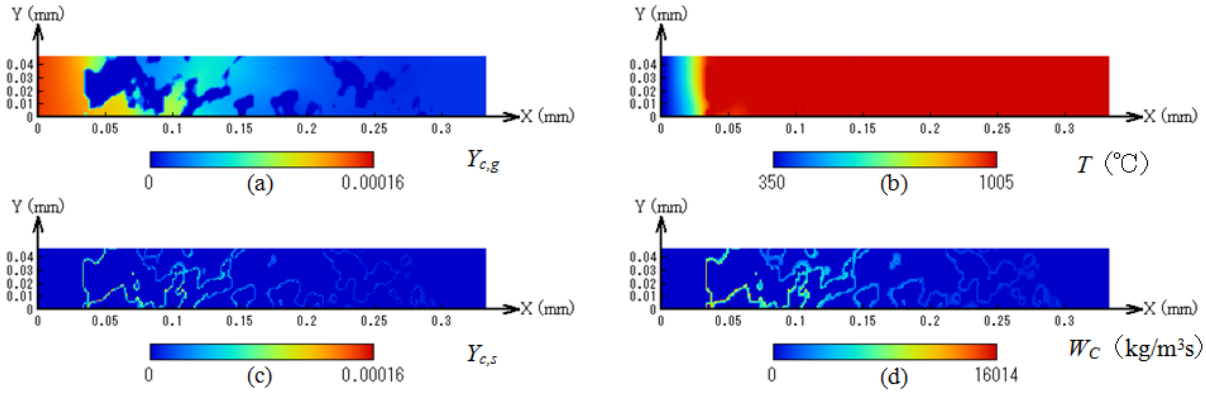

Fig. 8 Distributions of (a) soot mass fraction in gas phase, (b) temperature, (c) deposited soot, (d) reaction rate at t = 3.833s, T_w = 1000 K.

[Word Count] = (50+10)*2.2*2 + 27 (caption) = 291 words

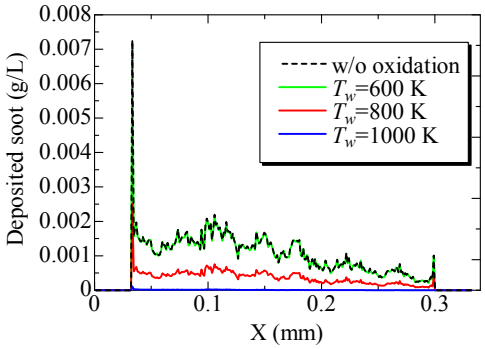

Fig. 9 Distribution of deposited soot at t =3.833 s.

[Word Count] = (45+10)*2.2*1 +10 (caption) = 131 words

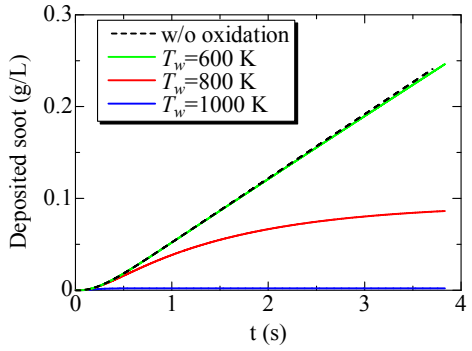

Fig. 10 Time-variation of deposited soot at different filter temperature.

[Word Count] = (45+10)*2.2*1 + 10 (caption) = 131 words